Engineering Science and Technology, an International Journal 40 (2023) 101364

HOSTED BY

Contents lists available at ScienceDirect

Engineering Science and Technology, an International Journal

journal homepage: www.elsevier.com/locate/jestch

A new capacitive coupler design for wireless capacitive power transfer applications

Mehmet Zahid Erel [a,*], Kamil Cagatay Bayindir [b], Mehmet Timur Aydemir [c]

[a] Department of Energy Systems Engineering, Ankara Yildirim Beyazit University, Ankara 06010, Turkey
[b] Department of Electrical and Electronics Engineering, Ankara Yildirim Beyazit University, Ankara 06010, Turkey
[c] Department of Electrical and Electronics Engineering, Kadir Has University, Istanbul 34083, Turkey

ARTICLE INFO

Article history:
Received 1 February 2022
Revised 6 July 2022
Accepted 12 February 2023
Available online 2 March 2023

Keywords:
Capacitive power transfer
Wireless charging
Capacitive coupler
External capacitors
Coupling capacitors

ABSTRACT

Capacitive power transfer (CPT) technology has become a promising alternative solution for wireless charging applications. This paper proposes a novel coupler design to form a resonant capacitor by inserting dielectric material between two bent metal plates for each primary and secondary circuit. The main purpose of the proposed coupler is to eliminate the external capacitors and solve the low coupling capacitance for CPT applications. A comparison to the conventional four-plate coupler is presented, which shows specifically higher coupling capacitance, lower required inductance, and lower cost. Finally, the effectiveness of the proposed coupler structure is verified by simulation and experimental results.

1. Introduction

1.1. Overview

Although inductive power transfer (IPT) systems dominate the wireless power transfer (WPT) technologies, recently capacitive power transfer (CPT) systems also have received significant attention due to their outstanding benefits such as negligible eddy-current loss, higher reliability, better misalignment performance, lower cost, lightweight, and lower EMI [1,2]. The CPT technology has many application areas in wireless charging concept. The LED lighting [3], portable device charging [4], biomedical devices [5], integrated circuits [6], and excitation of electric machines [7] may be shown as some of the examples for low transfer distance applications. The first example that comes to mind for large transfer distance applications is the wireless electric vehicle (EV) charging both for IPT and CPT systems [8,9]. Compensation topologies, converter topologies, and coupler structures play an essential role in the performance of CPT systems and therefore they should be designed carefully to obtain the desired power level to be competitive. In addition, the effects of dielectric materials on capacitive coupler structures have great importance for increasing the power transfer capability and electric field strength [10].

1.2. Literature survey

Filter-based topologies take crucial importance for compensation topologies. They reduce the required inductances and the number of resonant components. For instance, double-sided LCLC [11], double-sided CLLC [12], double-sided LCL [13], and double-sided LC [14] compensation topologies are suggested for electric vehicle (EV) charging applications. Furthermore, hybrid structures are put forward to enhance the misalignment performance, such as LC-CLC [15] and LCL-L [16].

Converter topologies also play a key role in CPT systems. A high-frequency inverter is utilized to enable AC waveform for the resonant devices at each side of the CPT system. The half-bridge, class E, and class D structures with reduced switching-device count typically used to obtain low cost, low loss, and relatively low size in CPT applications [17–19]. Besides, full-bridge inverter topology is mainly utilized to increase the power level in CPT applications [20]. Considering rectifier topologies, half-bridge [21], full-bridge [22], and active variable reactance (AVR) [23] structures have been proposed for high power CPT applications. On the other side, a class E rectifier topology has been proposed for low power CPT applications [24].

The capacitive coupler structure includes multiple metal plates to form an electric field that causes a displacement current to transfer power. Conventional capacitive coupler structures can be categorized into four types: two-plate, four-plate, six-plate, and

* Corresponding author.
E-mail address: mzerel@ybu.edu.tr (M.Z. Erel).

https://doi.org/10.1016/j.jestch.2023.101364
2215-0986/

electric field repeater. Chris Mi [25] discussed four-plate horizontal and vertical coupler structures for EV charging applications. Hence, the vertical coupler has better rotational misalignment capability than the horizontal coupler. Then, a coupler structure that comprises two metal plate is proposed for EV charging applications [26]. Herein, the chassis of a vehicle and earth ground are highlighted to substitute for two plates used in conventional four-plate structures. In addition, a two-plate capacitive coupler structure provides a decreased number of plates and cost reduction in CPT applications. However, the lower conductivity of earth ground is the drawback side. Then, Zhang et al., [27] proposed a six-plate coupler structure to provide less electric field emission for large transfer distance applications. Nevertheless, the number of coupling capacitances to realize the equivalent circuit and increased cost with six metal plates are the drawbacks. Zhang et al., [28] suggested the last conventional capacitive coupler structure called as an electric field repeater to enhance the transfer distance in CPT systems. However, the low system efficiency is the disadvantage of the coupler.

As well as conventional capacitive coupler structures, different designs are put forward for coupler structures in CPT applications. A conformal bumper structure is proposed to increase the coupling capacitance with a decreased transfer distance and increased surface area for electric vehicle charging applications [29]. However, the coupling capacitances are in the nanofarad ranges, and hence the transfer distance is limited to several millimeter ranges. Lu et al., [30] presented a hybrid coupler structure for portable device charging applications to use electric and magnetic fields simultaneously. However, two large external inductors are required to improve the equivalent inductances and to decrease the switching frequency. Regensburger et al., [31] presented a circular coupler structure with polytetrafluoroethylene (PTFE) enveloped not only to prevent arcing but also to increase energy transfer capability for high power applications. However, the divided inductors along with the coupler increase the complexity of the system for resonance condition. The combined coupler structures are suggested for CPT applications to provide space-saving [32], and to reduce fringing field level [33]. However, the CPT system becomes more complex to realize the equivalent circuit model.

1.3. Key contributions

Compared with the existing studies on CPT technology, the main contributions of this paper comprise the following: 1) A novel capacitive coupler structure is proposed to eliminate the external capacitors in CPT applications. 2) For the first time, four metal plates are bent, and PTFE dielectric materials are inserted between the bent sections to create an extra capacitance to replace the physical capacitor component, which is required for the resonance circuit. 3) As a conventional four-plate capacitive coupler structure, the capacitances between the same side plates form the main capacitances. Thanks to the proposed capacitive coupler structure, the role of main capacitances becomes more significant. 4) Due to the elimination of external capacitors for primary and secondary resonant circuits, reduced cost and space-saving are achieved in CPT systems. 5) The proposed capacitive coupler structure offers the opportunity to use different dielectric materials; thus, the power level can be drastically improved in CPT applications.

The rest of the paper is structured as follows. Section 2 highlights a conventional four-plate CPT system that consists of a conventional four-plate coupler structure and LC compensation topology. Along with the proposed capacitive coupler structure, operation principle, design, and analysis of the proposed four-plate CPT system are presented in Section 3. Section 4 presents a practical prototype of the proposed four-plate CPT system and together with a coupler comparison in terms of coupling capacitances between the conventional four-plate coupler structure and the proposed coupler structure. Moreover, the misalignment tests and electric field emissions are investigated in the proposed CPT system. Finally, conclusions and discussion are introduced in Section 5.

2. A conventional four-plate CPT system

2.1. Principles of conventional four-plate capacitive coupler structure

Plate design plays a key role in the determination of cross-coupling capacitances for CPT systems. A four-plate horizontal structure and hereafter called conventional four-plate coupler structure is shown in Fig. 1 and its parameter definitions are given in Table 1.

Fig. 2 depicts the four-plate capacitance model. In addition, the coupling capacitance term represents port and cross-coupling capacitance. Fig. 2(a) illustrates the port capacitance model of the conventional four-plate capacitive coupler structure. Herein, P_1 and P_2 show the transmitter side plates, P_3 and P_4 represent the receiver side plates. Since there are some port capacitances between the metal plates, there are a total of six equivalent port capacitances C_{T12}, C_{T13}, C_{T14}, C_{T23}, C_{T24}, and C_{T34}. Capacitances between the same side plates represent the self-capacitances of the capacitive coupler. The capacitances between the same sides are also known as main capacitances, C_{12} and C_{34}. Mutual capacitance is closely associated with the capacitances between both sides. Fig. 2(b) represents the cross-coupling capacitance model of the four-plate capacitive coupler structure. Here, C_{12}, C_{13}, C_{14}, C_{23}, C_{24}, and C_{34} present the cross-coupling capacitances. The equivalent π type model [34] and the equivalent two-port model [14] are put forward to simplify the complicated coupler structure. Among them, the π type model is demonstrated in Fig. 3.

In Fig. 3, C_P, C_S and C_M represent primary resonant capacitance, secondary resonant capacitance, and mutual capacitance, respectively. These capacitances are obtained using cross-coupling capacitances [13], as shown by

$$C_P = C_{12} + \frac{(C_{13}+C_{14}).(C_{23}+C_{24})}{C_{13}+C_{14}+C_{23}+C_{24}} \quad (1)$$

$$C_S = C_{34} + \frac{(C_{13}+C_{23}).(C_{14}+C_{24})}{C_{13}+C_{14}+C_{23}+C_{24}} \quad (2)$$

$$C_M = \frac{(C_{24}C_{13})-(C_{14}C_{23})}{C_{13}+C_{14}+C_{23}+C_{24}} \quad (3)$$

2.2. Circuit topology

The conventional four-plate coupler structure and LC compensation topology consist of the conventional four-plate CPT system as illustrated in Fig. 4. The role of the plates P_1 and P_2 is to transmit power wirelessly while the plates P_3 and P_4 serve to receive power.

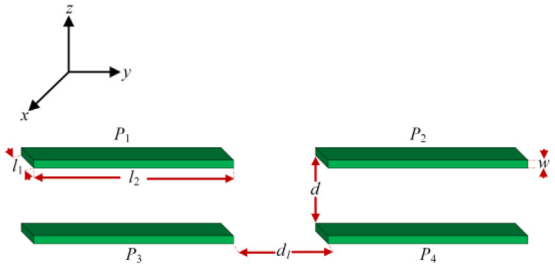

Fig. 1. A conventional four-plate coupler structure.

Table 1
Parameter definition of the conventional four-plate coupler structure.

Parameter	Definition
l_1	Plate length (x-direction)
l_2	Plate length (y-direction)
d	Transfer distance
d_1	Plate distance for primary/secondary sides
w	Plate thickness

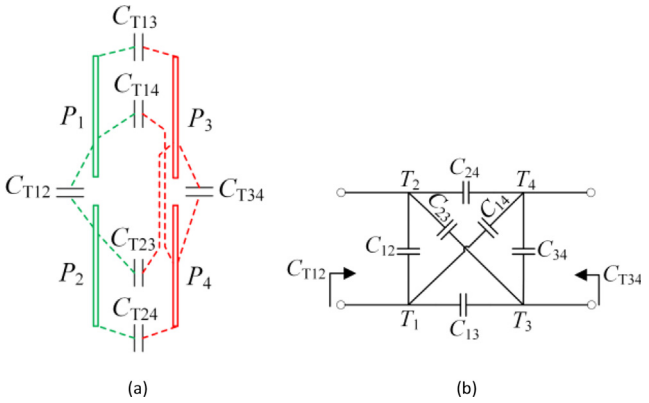

Fig. 2. Four plate capacitance model. (a) port capacitance model, (b) cross-coupling capacitance model.

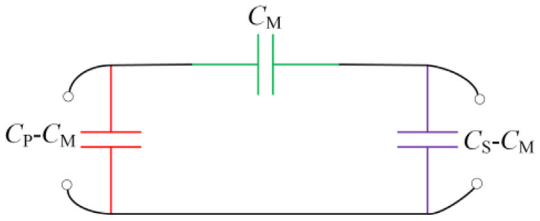

Fig. 3. Equivalent π type model.

In this concept, the full-bridge structure for the inverter is mainly utilized to excite the resonant circuit in the primary side. Resonant inductors and external capacitors are also used to resonate with the capacitive coupler structure for each side of the wireless charging system. Herein, the external capacitors are typically used due to low coupling capacitance of the system. For this reason, many problems occur, such as high cost, high loss, and space limitation. A full-bridge rectifier is utilized at the last side of the circuitry to provide a regulated output voltage.

3. Proposed four-plate CPT system

3.1. Proposed coupler structure

The proposed coupler structure is shown in Fig. 5 and its parameter definitions are given in Table 2. The proposed coupler aims to solve the low coupling capacitance of the CPT system. Low coupling capacitance condition creates problems and requirements such as high resonant inductance, high switching frequency, high cost, and low efficiency. For this reason, all four metal plates are bent, and a dielectric material is inserted between these bent pieces to create an extra capacitance to utilize for primary and secondary resonant circuits.

The value measured between each plate represents the port capacitance as depicted in Fig. 6. It is not mentioned as a value of cross-coupling capacitance. The cross-coupling capacitance model can be represented as in the general model of the conventional four-plate coupler structure depicted in Fig. 2(b). In addition, the Y-Δ and Δ-Y transformation theories are used to determine the cross-coupling capacitances based on Fig. 2(b) [35]. The port capacitances are derived using cross-coupling capacitances as given by Eq. (A.1). (For more details see Appendix A). Then, the cross-coupling capacitances are determined according to the port capacitances.

3.2. Circuit topology

The proposed coupler structure and LC compensation topology form the proposed four-plate CPT system as represented in Fig. 7. The bent sections with dielectric materials form the main capacitances for the resonant circuits at both sides. Then, the primary

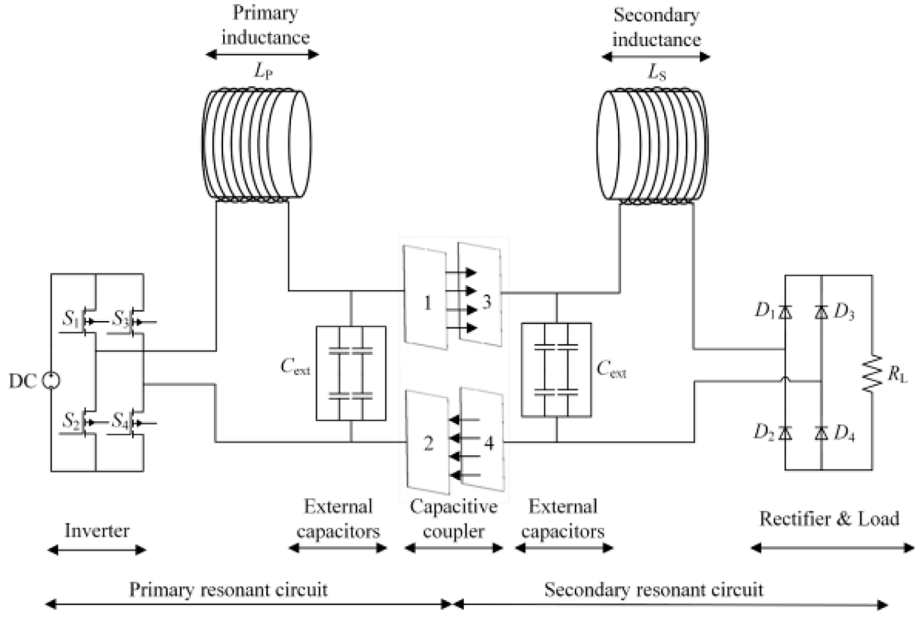

Fig. 4. Circuit topology of a conventional four-plate CPT system.

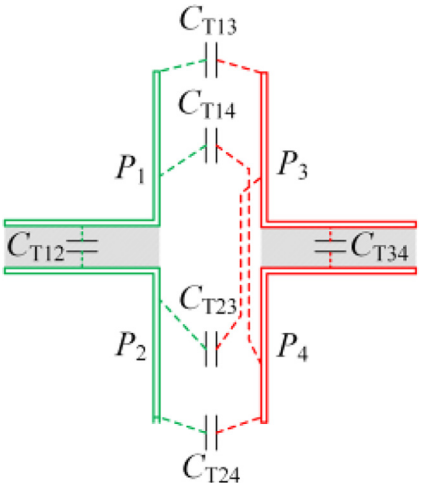

Fig. 5. Proposed coupler structure.

Table 2
Parameter definition of the proposed coupler structure.

Parameter	Definition
l_1	Plate length (x-direction)
l_2	Plate length (y-direction)
l_3	Plate length (z-direction)
l_4	Dielectric thickness
d	Transfer distance
w	Plate thickness

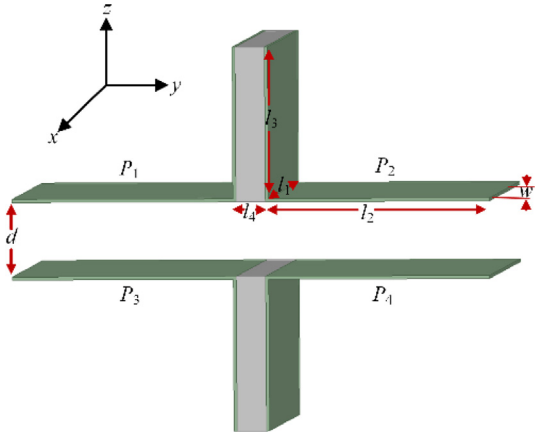

Fig. 6. Port capacitance model of the proposed coupler structure.

and secondary inductors resonate with the capacitive coupler structure to produce high voltages on metal plates and, to transfer power. Now that the bent sections constitute the main capacitances of the coupler, the inserted dielectric material becomes prominent to obtain the desired coupling capacitance and power level.

3.3. Operation principle

The equivalent circuit of the proposed four-plate CPT system with the π type model is demonstrated in Fig. 8. The full-bridge inverter is utilized to excite the resonant circuit. The LC compensation topology is then included in the system. Herein, L_P and L_S represent primary and secondary inductances, respectively. C_P and C_S

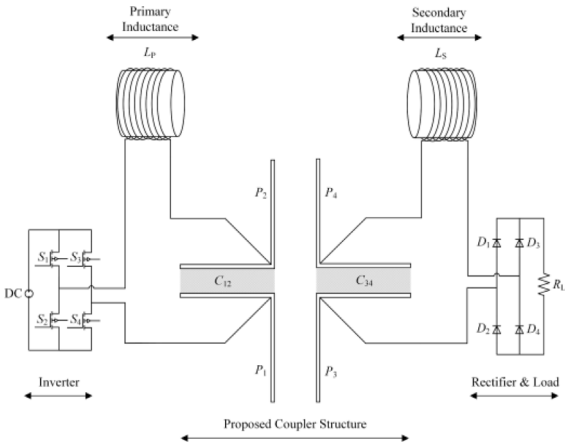

Fig. 7. Circuit topology of the proposed four-plate CPT system.

represent primary and secondary capacitances and C_M represents the equivalent mutual capacitance of the system, respectively. The full-bridge diode rectifier is utilized to supply DC current to the load. The fundamental harmonics approximation (FHA) method is utilized to understand the behaviour of the proposed coupler structure as depicted in Fig. 9 [34]. In addition, the superposition theorem is used to obtain the related parameters. Fig. 9(a) introduces the simplified resonant circuit model. Fig. 9(b) indicates the resonant circuit, which is excited by the output source, V_S and Fig. 9(c) represents the resonant circuit, which is excited by the input source, V_P. Herein, sinusoidal voltage sources are substitute for primary and secondary square voltage sources, V_P and V_S.

From Fig. 9(b), the primary resonant current is calculated as,

$$I_P = -\frac{C_S}{C_M} \cdot \frac{1}{jw_P L_P} \cdot V_S \tag{4}$$

From Fig. 9(c), the secondary resonant current is calculated as,

$$I_S = -\frac{C_P}{C_M} \cdot \frac{1}{jw_S L_S} \cdot V_P \tag{5}$$

Then, the coupling coefficient k_c is expressed as,

$$k_c = \frac{C_M}{\sqrt{C_P C_S}} \tag{6}$$

The resonant frequency of each side of the system is typically selected to be the same that defined as,

$$\omega_0 = \omega_P = \omega_S = \frac{1}{\sqrt{L_P \cdot C_P}} = \frac{1}{\sqrt{L_S \cdot C_S}} \tag{7}$$

The value of the coupling coefficient is typically much lower than 1. Thus, the output power can be roughly determined by,

$$P_{out} = |V_S| \cdot |I_S| \cong \frac{\omega_c \cdot C_M}{k_c^2} \cdot |V_P| \cdot |V_S| \tag{8}$$

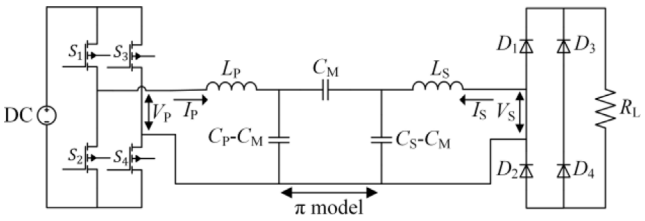

Fig. 8. Equivalent circuit of the proposed four-plate CPT system with the π type model.

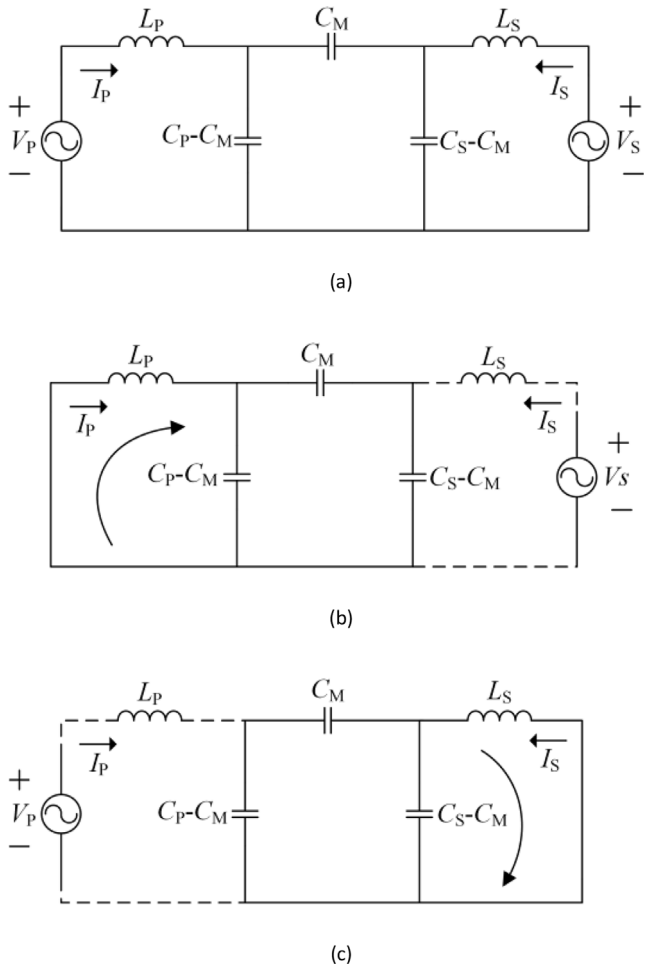

Fig. 9. The FHA analysis of the proposed four-plate CPT system (a) Simplified resonant circuit model, (b) Excited only by a secondary voltage source, (c) Excited only by a primary voltage source.

3.4. Design and analysis

This section introduces the design and analysis of the proposed four-plate CPT system. The design procedure of the proposed CPT system to determine the resonant components can be stated as follows: the port capacitances are firstly measured by an LCR meter. Then, the cross-coupling capacitances are determined according to the port capacitances, which are derived using the cross-coupling capacitance model. To solve high-order equations, Wolfram Mathematica software is utilized to obtain the cross-coupling capacitances. Depending on the obtained cross-coupling capacitances, the primary and secondary capacitances, and mutual capacitance are calculated. Afterwards, the primary and secondary inductances are determined based on the selected switching frequency for both sides.

To further prove that the proposed coupler structure is useful, a 60-V input, 60-V output, 110-W CPT system using LC compensation topology has been designed and tested. The four metal plates have been devised to be symmetric to simplify the procedure. The physical dimensions of the proposed coupler structure are given in Table 3. According to the selected coupler dimensions, the port capacitances are measured firstly, and the cross-coupling capacitances are then calculated using Eq. (A.1). The obtained results are given in Table 4. Afterwards, the values of compensation capacitors are determined using Eqs. (1), (2), and (3), respectively. The coupling coefficient is also determined by using Eq. (6). The values of compensation inductors are calculated based on the selected switching frequency using Eq. (7). Therefore, the circuit parameters of a designed four-plate CPT system are given in Table 5.

The PLEXIM Plecs software is preferred to examine the operation of the proposed four-plate CPT system. The voltage and current waveforms of the resonant circuits are depicted in Fig. 10. Fig. 10(a) shows the primary-side resonant voltage and current waveforms, and Fig. 10(b) represents the secondary-side resonant voltage and current waveforms. The current waveforms are scaled two times to better observe the resonance conditions at both sides. According to the simulation results, the efficient resonance condition is achieved for the designed CPT system.

4. Experimental setup and validations

4.1. Coupler validation

A comparative study is conducted between the conventional four-plate coupler structure and the proposed coupler structure considering coupling capacitances as shown in Fig. 11. Fig. 11(a) represents the experimental prototype of the conventional four-plate coupler structure, and Fig. 11(b) indicates the experimental prototype of the proposed coupler structure. Here, the four aluminum metal plates are used for both coupler structures. As a difference of the proposed coupler structure, the four aluminum metal plates are bent, and PTFE dielectric materials also known as Teflon are inserted between the bent sections. Additionally, a robust adhesive bandage is implemented for both dielectric materials and bent sections to avoid creating an air–gap. The PTFE is selected for its high dielectric strength feature of > 20 kV/mm when the air breakdown occurs at 3 kV/mm. Moreover, PTFE has a dielectric constant of 2.1, and hence it provides two times higher coupling capacitances than air, which has a dielectric constant of 1. PTFE has also a low dissipation factor at MHz frequency ranges [36].

The comparison study aims to show the contribution of the bent sections compared with the conventional four-plate coupler. To make a fair comparison, plate dimensions and transfer distance of conventional four-plate coupler structure are selected as same as the proposed coupler structure, which is given in Table 3. With the same switching frequency setting of 1 MHz, the coupling capacitances of the conventional four-plate coupler structure are obtained as given in Table 6. To determine the port and cross-coupling capacitances in the conventional four-plate coupler structure, the same procedure is utilized as the proposed coupler structure. Namely, the port capacitances are measured using an LCR meter. Then, the cross-coupling capacitances are determined according to the port capacitances, which are derived using the cross-coupling capacitance model, shown in Fig. 2(b). To solve high-order equations, Wolfram Mathematica software is used to determine the cross-coupling capacitances.

The obtained results show that there is a significant difference for each port and cross-coupling capacitances when comparing both couplers. The proposed four-plate coupler structure has

Table 3
Dimensions of the proposed coupler structure.

Parameter	Value
l_1	300 mm
l_2	150 mm
l_3	100 mm
l_4	1 mm
d	5 mm
w	2 mm

Table 4
Coupling capacitances of the proposed coupler structure.

Port capacitance	Value (pF)	Cross-coupling capacitance	Value (pF)
C_{T12}	291.23	C_{12}	247.27
C_{T13}	181.96	C_{13}	45.91
C_{T14}	163.90	C_{14}	3.72
C_{T23}	163.63	C_{23}	2.68
C_{T24}	188.49	C_{24}	46.58
C_{T34}	294.78	C_{34}	250.68

Table 5
Design values of the proposed four-plate CPT system.

Parameter	Value
C_P	424.87 pF
C_S	429.65 pF
C_M	34.63 pF
k_c	8.1 %
L_P	59.62 μH
L_S	58.96 μH
f_{sw}	1 MHz

Table 6
Coupling capacitances of the conventional four-plate coupler structure.

Port capacitance	Value (pF)	Cross-coupling capacitance	Value (pF)
C_{T12}	8.40	C_{12}	36.92
C_{T13}	79.08	C_{13}	92.23
C_{T14}	8.48	C_{14}	33.94
C_{T23}	8.12	C_{23}	35.11
C_{T24}	73.10	C_{24}	85.65
C_{T34}	8.97	C_{34}	41.19

posed coupler structure specifically contribute to the main capacitances. Therefore, the proposed coupler structure presents higher coupling capacitances and acts a key part to determine the resonant capacitance of the system. Additionally, the proposed coupler allows the use of different dielectric materials via its bent sections. Thus, the proposed four-plate coupler structure becomes more prominent providing higher coupling capacitances, higher power level, lower required inductance, lower cost, relatively higher transfer efficiency, and space-saving for CPT applications.

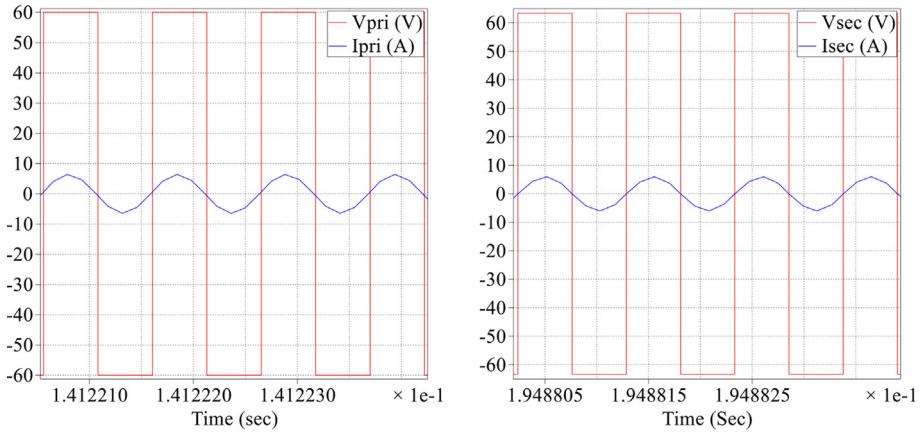

Fig. 10. Resonant voltage and current waveforms: (a) primary-side resonant voltage and current waveforms, (b) secondary-side resonant voltage and current waveforms.

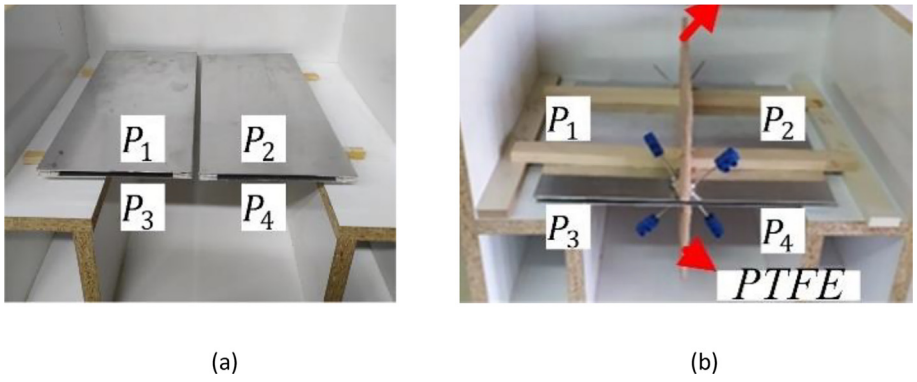

Fig. 11. Coupler structures: (a) the conventional four-plate coupler structure, (b) the proposed coupler structure.

higher port and cross-coupling capacitances via its bent sections. Among the coupling capacitances, C_{12} and C_{34} represent the main capacitances for both coupler structures. However, the main capacitances of the conventional four-plate coupler structure are lower than other coupling capacitances. The bent sections of the pro-

4.2. System performance validation

After the validity of the proposed coupler structure by experimental studies, a 110-W four-plate CPT system has been built with

a 33.1 Ω resistive load as shown in Fig. 12. The transfer distance is also set to 5 mm for E-mobility applications.

As a practical prototype of the proposed four-plate CPT system, the input voltage is set to 60 V, and the output voltage is measured at 50 V. The average input and output currents are obtained at 1.83 A and 1.51 A, respectively. Hence, a loosely-coupled four-plate CPT system with a coupling coefficient of 8.1 % is achieved with an efficiency of 68.76 %. Due to the mechanical design of the proposed coupler structure, there are small differences between the resonant components as given in Table 5. The air-core inductors are used for the resonant circuits to present a good performance in high-frequency applications. Furthermore, the resonant inductors are made with Litz-wire to provide reduced skin-effect and lower magnetic losses. The proposed coupler structure is fixed, and the port capacitances are measured by using a GW INSTEK LCR-8110G meter. Then, the cross-coupling capacitances are obtained using Wolfram Mathematica software according to the port capacitances. To generate PWM signals, STM32F4 Discovery Board is used for the designed CPT system. Silicon Carbide (SiC) MOSFETs C2M0080120D series from CREE are used to build the full-bridge inverter. As SiC diodes, IDH06G65C6XKSA1 series from INFINEON are preferred in passive rectifier bridge with a relatively low forward voltage of 1.25 V. The operating frequency is set to 1 MHz. PCB dimensions are designed as 10 × 10 cm for inverter and rectifier circuit topologies. The experimental waveforms of the resonant voltages and currents are depicted in Fig. 13. Fig. 13(a) demonstrates the primary-side resonant voltage and current waveforms, which represent inverter output voltage and current waveforms as well. Herein, the system achieves zero-voltage switching (ZVS) operation since inverter output current lags the voltage slightly. Fig. 13(b) depicts the secondary-side resonant voltage and current waveforms, which represent rectifier input voltage and current waveforms as well. Additionally, the in-phase operation is succeeded for secondary-side resonant voltage and current waveforms. As a consequence of the experimental study, there is a good harmony between the obtained results, which confirm the proposed coupler structure for CPT applications.

4.3. Misalignment test

The misalignment performance of the proposed four-plate CPT system is examined in this section. Thus, the prominent misalignment applications such as x-direction misalignment and z-direction misalignment or different transfer distances between each side of the system are considered in the practical concept.

The two key parameters as dc-dc system efficiency and output power are measured under misalignment conditions.

The x-direction misalignment is evaluated from 30 mm to 120 mm, which is about half of the capacitive coupler. As mentioned before, the transfer distance of the designed four-plate CPT system is 5 mm, and hence the variations of transfer distance are taken into account up to 9 mm in increments of 1 mm.

The changes in output power and dc-dc system efficiency of the proposed four-plate CPT system concerning x-direction misalignment are depicted in Fig. 14. Furthermore, the performance of the proposed four-plate CPT system in terms of these parameters associated with transfer distances is demonstrated in Fig. 15.

It was found that the output power and dc-dc efficiency of the proposed CPT system decrease with the misalignments. When the × misalignment is 30 mm, the dc-dc system efficiency and output power of the proposed four-plate CPT system decrease to 66.22 % and 71.52 W, respectively. In this condition, there is not a significant reduction in both system efficiency and output power. At 60 mm x-direction misalignment, the dc-dc system efficiency drops to 50.74 % and output power reduces to 50. 74 W, which is about 30% of the perfectly aligned system. When the misalignment in the x-direction increases from 60 mm to 120 mm, there is a noticeable reduction in the value of system efficiency and output power.

The different transfer distances are also evaluated in this concept. When the transfer distance increases to 6 mm, the system efficiency and output power of the proposed CPT system drop to nearly 30 % of the perfectly aligned system. When the transfer distance increases to 9 mm, the performance of the system is affected dramatically by virtue of the missed resonant frequency.

4.4. Electric field emission

Electric field emissions of the proposed four-plate CPT system are examined as depicted in Fig. 16. Thus, Narda EHP-200A Electric & Magnetic Field Analyzer (3 kHz-30 MHz) is used to evaluate the electric field strength of the proposed CPT system for different distances from the capacitive coupler.

According to the IEEE C95. 1 standard, the electric field strength ought to be lower than 640 V/m at 1 MHz operating frequency to provide the safety regulations [37]. Hence, different critical points are pointed out to observe the behaviour of system. At 300 mm distance from the capacitive coupler, the electric field strength of the proposed CPT system is obtained as 754.25 V/m, which is not compatible with the standard. The electric field strengths are obtained as 604.25 V/m and 574.67 V/m for 400 mm and 450 mm distances from the coupler, respectively. As a conclusion, the electric field strength of the proposed four-plate CPT system is compatible with the IEEE C95.1 standard around 400 mm away from the capacitive coupler.

5. Conclusions and discussion

This paper suggests a new capacitive coupler design for CPT applications. Four pieces of aluminum plates have been bent for the proposed coupler structure and PTFE dielectric materials are inserted between the bent sections. Besides design and analysis, a comparative study is conducted to confirm the effectiveness of the suggested coupler structure in terms of coupling capacitances against the conventional four-plate coupler structure. As a result of the comparison, higher coupling capacitances that represent port and cross-coupling capacitances are provided by the proposed coupler structure. After the validation of the proposed coupler, an experimental prototype of the four-plate CPT system is built. Thus, a 110-W wireless capacitive charging is succeeded over a transfer distance of 5 mm for E-mobility applications.

The performance of the proposed four-plate CPT system is also evaluated in terms of x-direction misalignment and different transfer distances. In compliance with the obtained results, the output power and dc-dc system efficiency reduce with both x misalignments and different transfer distances. The main reasons can be stated that the selected LC compensation topology under x misalignment applications and the missed resonant frequency for different transfer distances.

The electric field emissions are reviewed in the proposed CPT system. It is concluded that the safe area is provided after around 400 mm away from the capacitive coupler, which is compatible with the IEEE C95.1 standard.

Due to the bent section feature of the proposed coupler structure, the major advantages have been gained from the PTFE dielectric material that enables high dielectric strength and high relative permittivity. In addition, the values of resonant capacitors are drastically increased for the resonant circuits at both sides. At the same time, the required inductances are substantially decreased for the resonant circuits at both sides. Depending on the inserted dielectric material, the main capacitances of the cou-

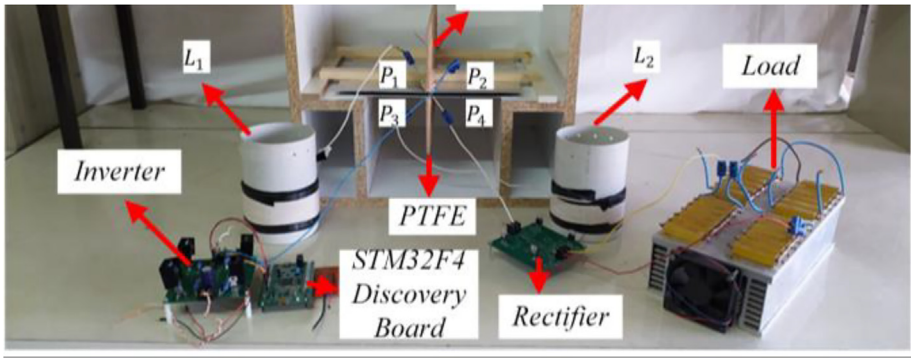

Fig. 12. Experimental prototype of the proposed four-plate CPT system.

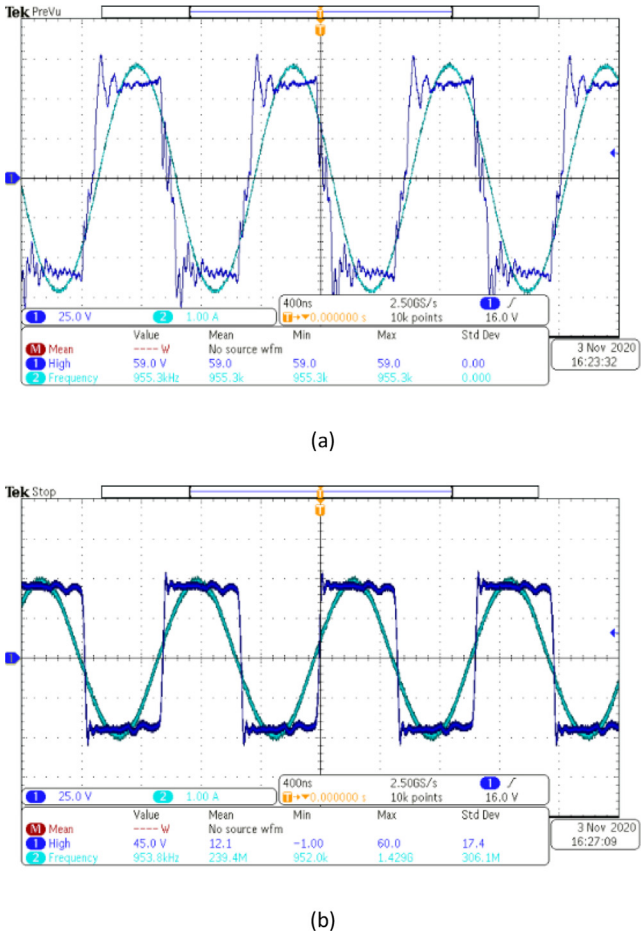

Fig. 13. Experimental waveforms of the resonant voltages and currents: (a) primary-side resonant voltage and current waveforms, (b) secondary-side resonant voltage and current waveforms.

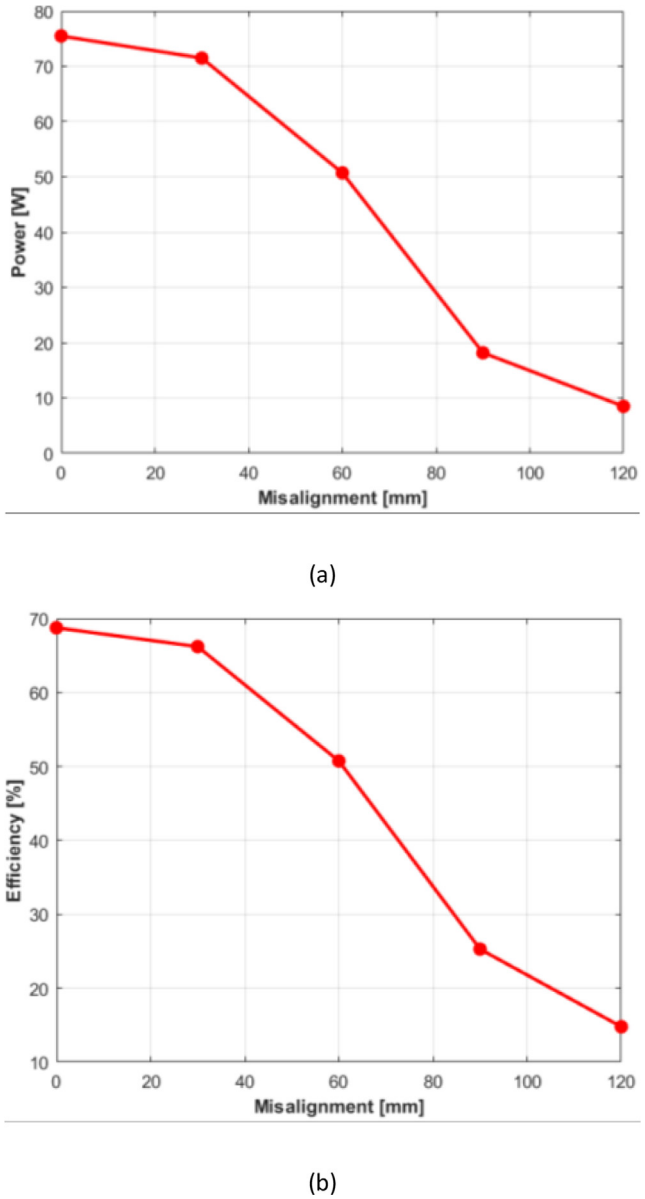

Fig. 14. The performance of the proposed four-plate CPT system under x-direction misalignment: (a) measured output power, (b) measured dc-dc system efficiency.

pler and hence the power transfer level can be increased. With the proposed coupler structure, the cost reduction is prominent for the proposed four-plate CPT system. The reduced cost is provided by the eliminated high-priced external capacitors and the reduced size of compensation inductors made with Litz-wire, which proofs the validity of the proposed coupler structure. The proposed coupler structure has also a flexible and ease of implementation feature and thus it is expected to make a great contribution by acting as a resonant capacitor for WPT applications.

Future directions of this research comprise testing different dielectric materials, and different coupler geometries for the proposed coupler structure to further decrease the system cost and improve the system efficiency.

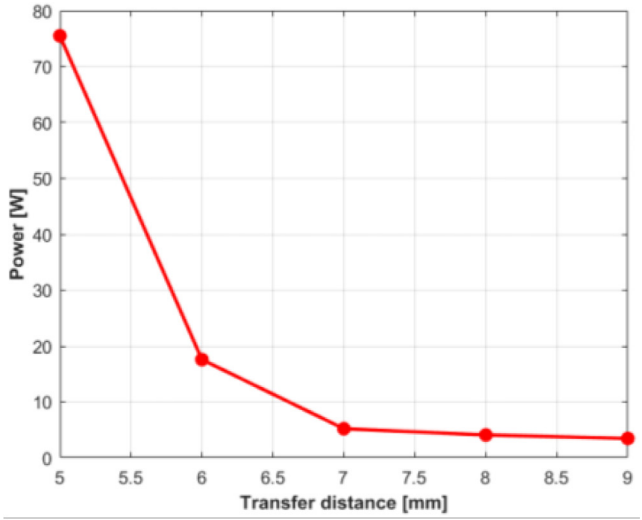

(a)

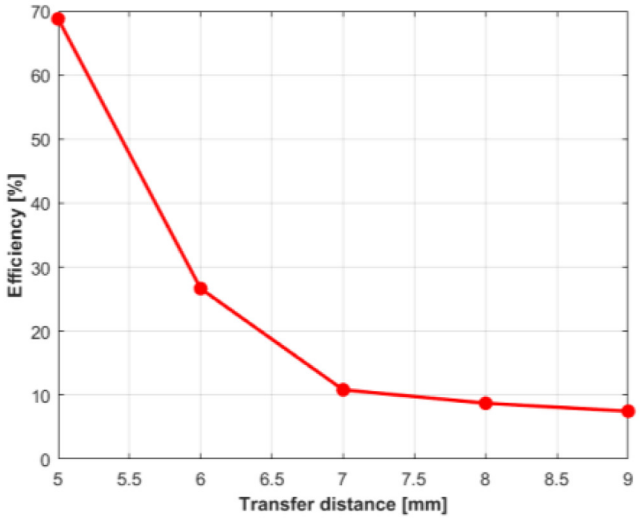

(b)

Fig. 15. The performance of the proposed four-plate CPT system for different transfer distances: (a) measured output power, (b) measured dc-dc system efficiency.

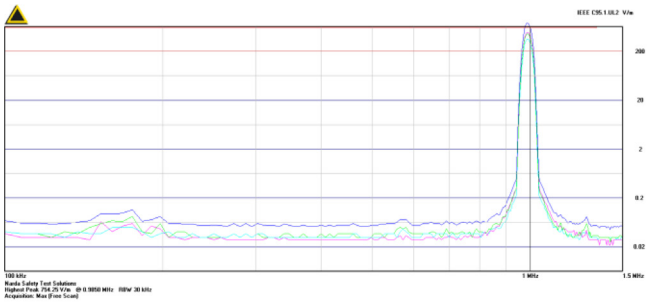

(a)

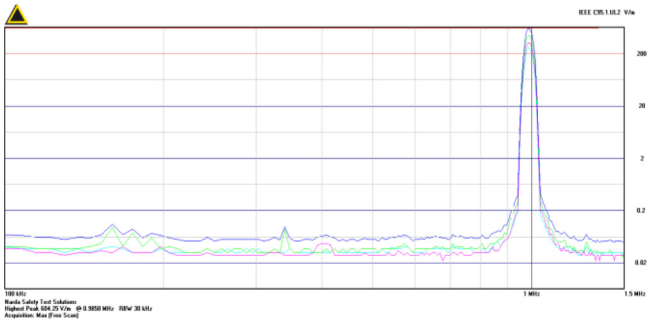

(b)

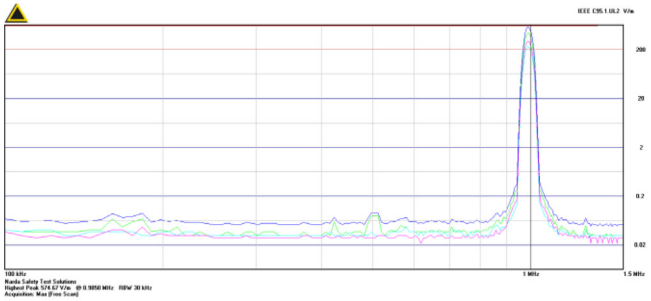

(c)

Fig. 16. Electric field emissions of the proposed four-plate CPT system for different distances: (a) at 350 mm, (b) at 400 mm, (c) at 450 mm.

Funding

This research did not receive any specific grant from funding agencies in the public, commercial, or not-for-profit sectors.

Declaration of Competing Interest

The authors declare that they have no known competing financial interests or personal relationships that could have appeared to influence the work reported in this paper.

Appendix A

Derivation of port capacitances using cross-coupling capacitances is given by,

$$C_{T12}=C_{12}+\frac{C_{14}C_{24}}{C_{14}+C_{24}+C_{34}}+\frac{\left(C_{13}+\frac{C_{14}C_{34}}{C_{14}+C_{24}+C_{34}}\right)\left(C_{23}+\frac{C_{24}C_{34}}{C_{14}+C_{24}+C_{34}}\right)}{C_{13}+C_{23}+\frac{C_{14}C_{34}}{C_{14}+C_{24}+C_{34}}+\frac{C_{24}C_{34}}{C_{14}+C_{24}+C_{34}}}$$

$$C_{T13}=C_{13}+\frac{C_{14}C_{34}}{C_{14}+C_{24}+C_{34}}+\frac{\left(C_{12}+\frac{C_{14}C_{24}}{C_{14}+C_{24}+C_{34}}\right)\left(C_{23}+\frac{C_{24}C_{34}}{C_{14}+C_{24}+C_{34}}\right)}{C_{12}+C_{23}+\frac{C_{14}C_{24}}{C_{14}+C_{24}+C_{34}}+\frac{C_{24}C_{34}}{C_{14}+C_{24}+C_{34}}}$$

$$C_{T14}=C_{14}+\frac{(C_{12}C_{13}+C_{12}C_{23}+C_{13}C_{23})\left(\frac{(C_{12}C_{13}+C_{12}C_{23}+C_{13}C_{23})C_{24}}{C_{13}\left(\frac{C_{12}C_{13}+C_{12}C_{23}+C_{13}C_{23}}{C_{13}}+C_{24}\right)}+\frac{(C_{12}C_{13}+C_{12}C_{23}+C_{13}C_{23})C_{34}}{C_{12}\left(\frac{C_{12}C_{13}+C_{12}C_{23}+C_{13}C_{23}}{C_{12}}+C_{34}\right)}\right)}{C_{23}\left(\frac{(C_{12}C_{13}+C_{12}C_{23}+C_{13}C_{23})}{C_{23}}+\frac{(C_{12}C_{13}+C_{12}C_{23}+C_{13}C_{23})C_{24}}{C_{13}\left(\frac{C_{12}C_{13}+C_{12}C_{23}+C_{13}C_{23}}{C_{13}}+C_{24}\right)}+\frac{(C_{12}C_{13}+C_{12}C_{23}+C_{13}C_{23})C_{34}}{C_{12}\left(\frac{C_{12}C_{13}+C_{12}C_{23}+C_{13}C_{23}}{C_{12}}+C_{34}\right)}\right)} \quad (A.1)$$

$$C_{T23}=C_{23}+\frac{C_{24}C_{34}}{C_{14}+C_{24}+C_{34}}+\frac{\left(C_{12}+\frac{C_{14}C_{24}}{C_{14}+C_{24}+C_{34}}\right)\left(C_{13}+\frac{C_{14}C_{34}}{C_{14}+C_{24}+C_{34}}\right)}{C_{12}+C_{13}+\frac{C_{14}C_{24}}{C_{14}+C_{24}+C_{34}}+\frac{C_{14}C_{34}}{C_{14}+C_{24}+C_{34}}}$$

$$C_{T24}=C_{24}+\frac{C_{12}C_{14}}{C_{12}+C_{13}+C_{14}}+\frac{\left(C_{23}+\frac{C_{12}C_{13}}{C_{12}+C_{13}+C_{14}}\right)\left(C_{34}+\frac{C_{13}C_{14}}{C_{12}+C_{13}+C_{14}}\right)}{C_{23}+C_{34}+\frac{C_{12}C_{13}}{C_{12}+C_{13}+C_{14}}+\frac{C_{13}C_{14}}{C_{12}+C_{13}+C_{14}}}$$

$$C_{T34}=C_{34}+\frac{C_{13}C_{14}}{C_{12}+C_{13}+C_{14}}+\frac{\left(C_{23}+\frac{C_{12}C_{13}}{C_{12}+C_{13}+C_{14}}\right)\left(C_{24}+\frac{C_{12}C_{14}}{C_{12}+C_{13}+C_{14}}\right)}{C_{23}+C_{24}+\frac{C_{12}C_{13}}{C_{12}+C_{13}+C_{14}}+\frac{C_{12}C_{14}}{C_{12}+C_{13}+C_{14}}}$$

References

[1] F. Lu, H. Zhang, C. Mi, A review on the recent development of capacitive wireless power transfer technology, Energies 10 (2017), https://doi.org/10.3390/en10111752.

[2] C. Liu, A.P. Hu, Steady state analysis of a capacitively coupled contactless power transfer system, 2009 IEEE Energy Convers, Congr. Expo. ECCE 2009 (2009) 3233–3238, https://doi.org/10.1109/ECCE.2009.5316216.

[3] H.W.R. Liang, C.K. Lee, S.Y.R. Hui, Design, analysis, and experimental verification of a ball-joint structure with constant coupling for capacitive wireless power transfer, IEEE, J. Emerg. Sel. Top. Power Electron. 8 (2020) 3582–3591, https://doi.org/10.1109/JESTPE.2019.2938226.

[4] M. Kline, I. Izyumin, B. Boser, S. Sanders, Capacitive power transfer for contactless charging, Conf. Proc. – IEEE Appl. Power Electron. Conf. Expo. – APEC (2011) 1398–1404, https://doi.org/10.1109/APEC.2011.5744775.

[5] R. Sedehi, D. Budgett, J. Jiang, X. Ziyi, X. Dai, A.P. Hu, D. McCormick, A Wireless Power Method for Deeply Implanted Biomedical Devices via Capacitively Coupled Conductive Power Transfer, IEEE Trans. Power Electron. 36 (2021) 1870–1882, https://doi.org/10.1109/TPEL.2020.3009048.

[6] L. Chen, J. Sankman, R. Mukhopadhyay, M. Morgan, D.B. Ma, 25.1 A 50.7% peak efficiency subharmonic resonant isolated capacitive power transfer system with 62mW output power for low-power industrial sensor interfaces, in: 2017 IEEE Int. Solid-State Circuits Conf., IEEE, 2017: pp. 428–429. 10.1109/ISSCC.2017.7870444

[7] J. Dai, S. Hagen, D.C. Ludois, I.P. Brown, Synchronous Generator Brushless Field Excitation and Voltage Regulation via Capacitive Coupling through Journal Bearings, IEEE Trans. Ind. Appl. 53 (2017) 3317–3326, https://doi.org/10.1109/TIA.2017.2681621.

[8] S. Maji, S. Sinha, K.K. Afridi, Theoretical Limits of Power Transfer in Capacitive Wireless Charging Systems, 2020 IEEE 21st Work, Control Model. Power Electron. COMPEL 2020 (2020), https://doi.org/10.1109/COMPEL49091.2020.9265824.

[9] S. Li, J. Zhao, W. Tan, C. You, Optimal secure transmit design for wireless information and power transfer in V2X vehicular communication systems, AEU – Int. J. Electron. Commun. 118 (2020), https://doi.org/10.1016/j.aeue.2020.153148 153148.

[10] D. Vincent, S.S. Williamson, Role of dielectrics in the capacitive wireless power transfer system, Proc. IEEE Int. Conf. Ind. Technol. (2020-Febru (2020)) 1217–1222, https://doi.org/10.1109/ICIT45562.2020.9067136.

[11] F. Lu, H. Zhang, H. Hofmann, C. Mi, A Double-Sided LCLC-Compensated Capacitive Power Transfer System for Electric Vehicle Charging, IEEE Trans. Power Electron. 30 (2015) 6011–6014, https://doi.org/10.1109/TPEL.2015.2446891.

[12] F. Lu, H. Zhang, H. Hofmann, C. Mi, A,, CLLC-compensated high power and large air-gap capacitive power transfer system for electric vehicle charging applications, Conf. Proc. – IEEE Appl. Power Electron. Conf. Expo. – APEC. (2016-May (2016)) 1721–1725, https://doi.org/10.1109/APEC.2016.7468099.

[13] H. Zhang, F. Lu, H. Hofmann, W. Liu, C.C. Mi, A Four-Plate Compact Capacitive Coupler Design and LCL-Compensated Topology for Capacitive Power Transfer in Electric Vehicle Charging Application, IEEE Trans. Power Electron. 31 (2016) 8541–8551, https://doi.org/10.1109/TPEL.2016.2520963.

[14] F. Lu, H. Zhang, H. Hofmann, C.C. Mi, A Double-Sided LC-Compensation Circuit for Loosely Coupled Capacitive Power Transfer, IEEE Trans. Power Electron. 33 (2018) 1633–1643, https://doi.org/10.1109/TPEL.2017.2674688.

[15] B. Luo, R. Mai, L. Guo, D. Wu, Z. He, LC–CLC compensation topology for capacitive power transfer system to improve misalignment performance, IET Power Electron. 12 (2019) 2626–2633, https://doi.org/10.1049/iet-pel.2018.5606.

[16] V.B. Vu, M. Dahidah, V. Pickert, V.T. Phan, An improved LCL-L Compensation Topology for Capacitive Power Transfer in Electric Vehicle Charging, IEEE Access 8 (2020) 27757–27768, https://doi.org/10.1109/ACCESS.2020.2971961.

[17] D. Vincent, S.S. Williamson, A. Modeling, Design, and Verification of a Reduced Model Capacitive Power Transfer Based Wireless Charging System, ECCE, IEEE Energy Convers Congr. Expo. 2020 (2020) 4118–4123, https://doi.org/10.1109/ECCE44975.2020.9236285.

[18] L. Huang, A.P. Hu, Power Flow Control of Capacitive Power Transfer by Soft Switching of Extra Capacitors in Class e Converter, 2018 IEEE 4th South, Power Electron. Conf. SPEC 2019 (2018) 1–5, https://doi.org/10.1109/SPEC.2018.8635634.

[19] K.H. Yi, 6.78MHz capacitive coupling wireless power transfer system, J. Power Electron. 15 (2015) 987–993, https://doi.org/10.6113/JPE.2015.15.4.987.

[20] H. Zhang, C. Zhu, F. Lu, Long-Distance and High-Power Capacitive Power Transfer based on the Double-Sided LC Compensation: Analysis and Design, ITEC 2019–2019 IEEE Transp. Electrif. Conf. Expo. (2019) 5–9, https://doi.org/10.1109/ITEC.2019.8790595.

[21] S. Li, Z. Liu, H. Zhao, L. Zhu, C. Shuai, Z. Chen, Wireless Power Transfer by Electric Field Resonance and Its Application in Dynamic Charging, IEEE Trans. Ind. Electron. 63 (2016) 6602–6612, https://doi.org/10.1109/TIE.2016.2577625.

[22] B. Regensburger, K.K. Afridi, Challenges and Solutions to Passive Rectification in Multi-MHz Frequency Capacitive Wireless Power Transfer Systems for Electric Vehicle Charging, ECCE 2020 – IEEE Energy Convers. Congr. Expo. (2020) 5482–5486. 10.1109/ECCE44975.2020.9236085

[23] S. Sinha, A. Kumar, K.K. Afridi, Active variable reactance rectifier — A new approach to compensating for coupling variations in wireless power transfer systems, in: 2017 IEEE 18th Work. Control Model. Power Electron., IEEE, 2017: pp. 1–8. 10.1109/COMPEL.2017.8013348

[24] H. Ueda, H. Koizumi, Class-E DC-DC Converter with Basic Class-E Inverter and Class-E ZCS Rectifier for Capacitive Power Transfer, IEEE Trans Circuits Syst. II Express Briefs. 67 (2020) 941–945, https://doi.org/10.1109/TCSII.2020.2981131.

[25] C. Mi, High power capacitive power transfer for electric vehicle charging applications, 2015 6th Int Conf. Power Electron. Syst. Appl. Electr. Transp. - Automotive, Vessel Aircraft, PESA 2015 (2016) 1–4, https://doi.org/10.1109/PESA.2015.7398937.

[26] F. Lu, H. Zhang, C. Mi, A Two-Plate Capacitive Wireless Power Transfer System for Electric Vehicle Charging Applications, IEEE Trans. Power Electron. 33 (2018) 964–969, https://doi.org/10.1109/TPEL.2017.2735365.

[27] H. Zhang, F. Lu, H. Hofmann, W. Liu, C.C. Mi, Six-Plate Capacitive Coupler to Reduce Electric Field Emission in Large Air-Gap Capacitive Power Transfer, IEEE Trans. Power Electron. 33 (2018) 665–675, https://doi.org/10.1109/TPEL.2017.2662583.

[28] H. Zhang, F. Lu, H. Hofmann, C. Mi, An LC compensated electric field repeater for long distance capacitive power transfer, ECCE 2016 - IEEE Energy Convers. Congr. Expo. Proc. (2016) 1–5. 10.1109/ECCE.2016.7854858

[29] J. Dai, D.C. Ludois, Wireless electric vehicle charging via capacitive power transfer through a conformal bumper, Conf, Proc. – IEEE Appl. Power Electron. Conf. Expo. - APEC. 2015-May (2015) 3307–3313, https://doi.org/10.1109/APEC.2015.7104827.

[30] F. Lu, H. Zhang, H. Hofmann, C. Mi, An inductive and capacitive integrated coupler and its LCL compensation circuit design for wireless power transfer, ECCE 2016 - IEEE Energy Convers. Congr. Expo. Proc. (2016) 1–5. 10.1109/ECCE.2016.7854850

[31] B. Regensburger, J. Estrada, A. Kumar, S. Sinha, Z. Popovic, K.K. Afridi, High-Performance Capacitive Wireless Power Transfer System for Electric Vehicle Charging with Enhanced Coupling Plate Design, 2018 IEEE Energy Convers, Congr. Expo. ECCE 2018 (2018) 2472–2477, https://doi.org/10.1109/ECCE.2018.8557881.

[32] X. Gao, C. Liu, H. Zhou, W. Hu, Y. Huang, Y. Xiao, Z. Lei, J. Chen, Design and Analysis of a New Hybrid Wireless Power Transfer System with a Space-Saving Coupler Structure, IEEE Trans. Power Electron. 36 (2021) 5069–5081, https://doi.org/10.1109/TPEL.2020.3027473.

[33] S. Maji, S. Sinha, B. Regensburger, F. Monticone, K.K. Afridi, Reduced-Fringing-Field Multi-MHz Capacitive Wireless Power Transfer System Utilizing a Metasurface-based Coupler, 2020 IEEE 21st Work, Control Model. Power Electron. COMPEL 2020 (2020), https://doi.org/10.1109/COMPEL49091.2020.9265739.

[34] H. Zhang, F. Lu, H. Hofmann, C. Mi, A loosely coupled capacitive power transfer system with LC compensation circuit topology, ECCE 2016 - IEEE Energy Convers. Congr. Expo. Proc. (2016) 1–5. 10.1109/ECCE.2016.7854702

[35] X. Wu, Y. Su, X. Hou, X. Qing, X. Dai, Study on load adaptation of capacitive power transfer system with a four-plate compact capacitive coupler, Electr. Eng. 101 (2019) 733–742, https://doi.org/10.1007/s00202-019-00820-x.

[36] I. Beverte, U. Cabulis, S. Gaidukovs, Polytetrafluoroethylene films in rigid polyurethane foams' dielectric permittivity measurements with a one-side access capacitive sensor, Polymers (Basel). 13 (2021), https://doi.org/10.3390/polym13071173.

[37] IEEE Standard for Safety Levels with Respect to Human Exposure to Electric, Magnetic, and Electromagnetic Fields, 0 Hz to 300 GHz, in IEEE Std C95.1-2019 (Revision of IEEE Std C95.1-2005/Incorporates IEEE Std C95.1-2019/Cor 1-2019) , vol., no., pp.1-312, 4 Oct. 2019, 10.1109/IEEESTD.2019.8859679.